Deep machine learning potential for atomistic simulation of Fe-Si-O systems under Earth's outer core conditions

Chao Zhang,[1] Ling Tang,[2] Yang Sun,[3,4] Kai-Ming Ho,[3] Renata M. Wentzcovitch,[4] and Cai-Zhuang Wang[3,*]

[1]*Department of Physics, Yantai University, Yantai 264005, China*

[2]*Department of Applied Physics, College of Science, Zhejiang University of Technology, Hangzhou 310023, China*

[3]*Department of Physics and Astronomy, Iowa State University, Ames, Iowa 50011, USA*

[4]*Department of Applied Physics and Applied Mathematics, Columbia University, New York, New York 10027, USA*

(Received 17 January 2022; revised 20 April 2022; accepted 18 May 2022; published 7 June 2022)

Using artificial neural-network machine learning (ANN-ML) to generate interatomic potentials has been demonstrated to be a promising approach to address the longstanding challenge of accuracy vs efficiency in molecular dynamics (MD) simulations. Here, taking the Fe-Si-O system as a prototype, we show that accurate and transferable ANN-ML potentials can be developed for reliable MD simulations of materials at high-pressure and high-temperature conditions of the Earth's outer core. The ANN-ML potential for the Fe-Si-O system is trained by fitting the energies and forces of related binaries and ternary liquid structures at high pressures and temperatures obtained by first-principles calculations based on density functional theory (DFT). We show that the generated ANN-ML potential describes well the structure and dynamics of liquid phases of this complex system. In addition to binary systems ($Fe_{189}Si_{61}$, $Fe_{189}O_{61}$, and $Si_{80}O_{160}$) and ternary systems ($Fe_{189}Si_{38}O_{23}$), whose snapshots are included in the training dataset, the reliability of the ANN-ML potential is validated in two other ternary systems ($Fe_{189}Si_{23}O_{38}$ and $Fe_{158}Si_{14}O_{28}$), whose snapshots are not included in the training dataset. The efficient ANN-ML potential with DFT accuracy provides a promising scheme for accurate atomistic simulations of structures and dynamics of the complex Fe-Si-O system in the Earth's outer core.

DOI: 10.1103/PhysRevMaterials.6.063802

I. INTRODUCTION

Molecular dynamics (MD) simulation has been demonstrated to be a very useful computational tool for investigating the structure and dynamics at an atomistic level of detail for many systems in condensed matter physics, materials science, chemical and biological science, as well as earth science [1,2]. However, to perform reliable MD simulations, accurate and efficient descriptions of interatomic forces are critical.

Quantum mechanics calculations based on first-principles density functional theory (DFT) can provide an accurate description of interatomic forces and total energies for many materials, and *ab initio* MD (AIMD) simulations based on DFT have been successful in studying the structures and dynamics of many materials [3,4]. However, due to the heavy computational workload, AIMD can usually only be performed with a small simulation cell size (usually <500 atoms) and shorter time (typically <1 ns) even with advanced supercomputers.

To overcome time length and system size limitations in MD simulations, considerable efforts in the past several decades have been devoted to developing empirical interatomic potentials for MD simulations of various classes of materials. Conventionally, such interatomic potentials are modeled by given mathematical functions with respect to atomic coordinates in the systems and contain some empirical parameters to be fitted to the data from experimental measurement or first-principles calculations. Prototype interatomic potentials include Lennard-Jones potentials for noble gas and colloidal systems [5,6], Tersoff and Stillinger-Weber potentials [7,8] for covalent systems such as silicon and carbon, and embedded-atom method potentials [9] for the metallic systems. Although these potentials have been widely used in MD simulations and have produced many useful results for better understanding the structures and properties of materials [10,11], limitations for their application in more complex systems and/or under extreme environments have also been noticed. In many cases, reliable MD simulations for such complex systems are highly desirable when direct experimental studies become very difficult. For example, the Earth's outer core is believed to be composed of a liquid iron alloy with up to 10% of light elements such as silicon, oxygen, sulfur, carbon, or hydrogen. Despite extensive studies, chemical compositions and structures of the Earth's outer core are still elusive. Owing to the great pressures (135–363 GPa) and temperatures (3800–6500 K), experimental studies at core conditions are also limited. While MD simulations would provide useful insights into these problems, it is a great challenge to model interatomic potentials for such complex systems to ensure reliable MD simulations.

Due to the high dimensionality and many-body character of the interatomic potentials, it would be very difficult to choose appropriate mathematical functions for interatomic potentials based on chemical and physical intuition to de-

*wangcz@ameslab.gov

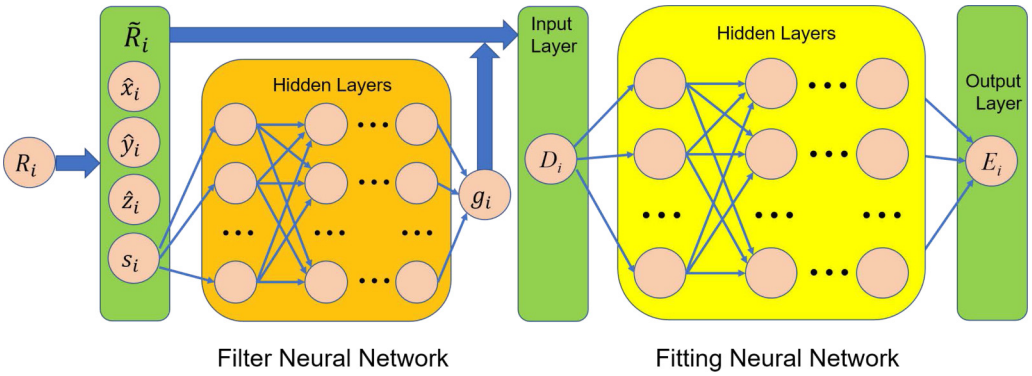

FIG. 1. Schematic illustration of the deep learning method for generating artificial neural-network machine learning (ANN-ML) interatomic potentials.

scribe the complicated interactions correctly and efficiently in complex materials [12]. On the other hand, machine learning (ML) is well-known for its ability to learn complex and highly nonlinear functional dependence. Artificial neural networks (ANNs) are universal continuous function approximators which provide an efficient way of interpolating high-dimensional functions. Interatomic potential fitting can be well suited for an ANN-ML method without assuming any mathematical functions. Within this spirit, considerable efforts in the last several years have been devoted to the development of ML interatomic potentials for MD simulations of various materials [13–33]. Among various ML interatomic potentials schemes, a deep-learning-based ANN proposed by Behler and Parrinello [13] and further improved by Wang *et al.* [29] and Zhang *et al.* [30–32] has been demonstrated to be very robust for reliable MD simulations of structures and behaviors of many complex materials [34–40].

In this paper, we develop an ANN-ML interatomic potential for the Fe-Si-O system, aimed at enabling accurate MD simulation of materials containing these three elements at extreme conditions of high pressure and high temperature like that in the Earth's outer core. We show that the developed ANN-ML interatomic potential describes well the structure and dynamics of the Fe-Si-O system at high pressure (>100 GPa) and high temperature (>3000 K). The potential will enable accurate and efficient atomistic simulations of structures and dynamics of complex Fe-Si-O systems in the Earth's outer core with many atoms and longer simulation time.

The paper is organized as follows. In Sec. II, we describe the datasets and the detailed process and parameters used in the ANN-ML training. The training and testing accuracies in comparison with the first-principles DFT results are also discussed. Application of the developed Fe-Si-O ANN-ML potential to MD simulation studies of the structures and dynamics of Fe-Si and Fe-O binaries and Fe-Si-O ternaries at high-temperature liquid phases are presented in Secs. III and IV, respectively. Comparisons with available *ab initio* MD simulations are also discussed. Finally, a summary is given in Sec. V.

II. DEVELOPMENT OF ANN-ML POTENTIAL FOR Fe-Si-O SYSTEM

An ANN contains three types of layers: an input layer, hidden layers, and an output layer. Each layer encompasses a set of artificial neurons termed a *node*, which linearly combines its inputs and then passes it through an activation function. To model the interatomic potential by the ANN, the input layer receives the data of atomistic structures, and the output layer generates the atomistic energy E_i on each atom. The total potential energy E of an atomistic structure is the sum of the atomistic energy $E = \sum_i E_i$. In this paper, we used the DEEPPOT-SE model as implemented in the DEEPMD-KIT package to develop the ANN-ML interatomic potential. It has been demonstrated that it is very robust in developing interatomic potentials for MD simulation studies of liquid and crystalline bulk structures and organic molecules.

There are two steps to construct E_i. First, the relative Cartesian coordinates $\{R_j\}$ of the neighboring atom j within a cutoff radius r_c with respect to atom i are transferred to the generalized coordination $\{\tilde{R}_i\}$ as

$$\{R_i\} = \{x_{ji}, y_{ji}, z_{ji}\} \rightarrow \{\tilde{R}_i\} = \{s(r_{ji}), \hat{x}_{ji}, \hat{y}_{ji}, \hat{z}_{ji}\},$$

where $\hat{x}_{ji} = s(r_{ji})x_{ji}/r_{ji}$, $\hat{y}_{ji} = s(r_{ji})y_{ji}/r_{ji}$, and $\hat{z}_{ji} = s(r_{ji})z_{ji}/r_{ji}$, have the angular information of the local environment. Here, $s(r_{ji})$ contains the radial information, defined as

$$s(r_{ji}) = \begin{cases} \frac{1}{r_{ji}}, & r_{ji} < r_{cs} \\ \frac{1}{r_{ji}}\left[\frac{1}{2}\cos\left(\pi \frac{r_{ji}-r_{cs}}{r_c-r_{cs}}\right) + \frac{1}{2}\right], & r_{cs} < r_{ji} < r_c, \\ 0, & r_{ji} > r_c \end{cases}$$

where r_{cs} is the smooth cutoff parameter. The radial information $s(r_{ji})$ is fed as an input into a local embedding neural network (called a *filter NN*). The output of the filter NN serving as weight coefficients to the generalized coordination $\{\tilde{R}_i\}$ will generate the local structure descriptor $\{D_i\}$, which contains translational, rotational, and permutational symmetries of the environment. Second, the local structure descriptor $\{D_i\}$ is transferred to atomistic energy E_i through a deep and forward neural network (called a *fitting NN*) which contains multiple hidden layers. The schematic illustration of constructing the ANN-ML interatomic potential is shown in Fig. 1.

The training process is a procedure of optimizing the parameters in filter and fitting NN using the Adam stochastic gradient decent method [41] with a family of loss functions [29]:

$$L(p_\varepsilon, p_f, p_\xi) = p_\varepsilon |\Delta\varepsilon|^2 + \frac{p_f}{3N}|\Delta F_i|^2 + \frac{p_\xi}{9}\|\Delta\xi\|^2,$$

TABLE I. The training datasets used for the Fe-Si-O ANN-ML potential development. The RMSE of energy and force predicted by the ANN-ML model are the validation RMSE.

System	Total number of atoms	Total number of snapshots	Density (g/cm^3)	Energy RMSE (meV/atom)	Force RMSE (eV/Å)
$Fe_{189}Si_{38}O_{23}$	250	23 143	8.36–10.65	5.3	0.43
$Fe_{189}Si_{61}$	250	29 967	9.63–9.93	4.7	0.39
$Fe_{189}O_{61}$	250	31 906	8.79–10.49	6.0	0.47
$Si_{80}O_{160}$	240	19 283	4.98–6.19	5.4	0.31
Fe	256	20 156	10.26–11.28	4.5	0.42

where Δ denotes the difference between the ANN-ML predictions and the DFT results. Here, N is the total number of atoms in the structure, ε is the energy per atom, F_i is the force on the atom i, and ξ is the virial tensor divided by N. The prefactors p_ε, p_f, and p_ξ are free to change during the training process.

The DEEPPOT-SE model in the DEEPMD-KIT package [29] is applied in the training process to develop the ANN-ML potential for the Fe-Si-O system. The cutoff radius (r_c) of the model is set to 6.5 Å, and descriptors decay smoothly from 6.0 Å (r_{cs}) to the cutoff radius of 6.5 Å. The size of the filter and fitting neural networks are (60, 120) and (240, 240, 240), respectively. A skip connection is built (ResNet) between two neighboring fitting layers [42]. The hyperbolic tangent is used as the nonlinear activation function. The learning rate decreases exponentially with respect to the starting value of 0.001. The ANN is initialized with random numbers, and the total number of training steps is 3 000 000. The decay rate and decay step are set to 0.96 and 10 000, respectively. In addition, the prefactors in the loss functions are $p_\varepsilon^{\text{start}} = 0.1$, $p_\varepsilon^{\text{limit}} = 0.1$, $p_f^{\text{start}} = 1000$, $p_f^{\text{limit}} = 1$, $p_\xi^{\text{start}} = 0$, and $p_\xi^{\text{limit}} = 0$.

The dataset used to train the ANN-ML interatomic potential for the Fe-Si-O ternary system consists of high-temperature and high-pressure liquids of pure Fe and related binaries and ternary, as listed in Table I. These data are generated by AIMD simulations and consist of potential energies for each structure and force on every atom in the structures.

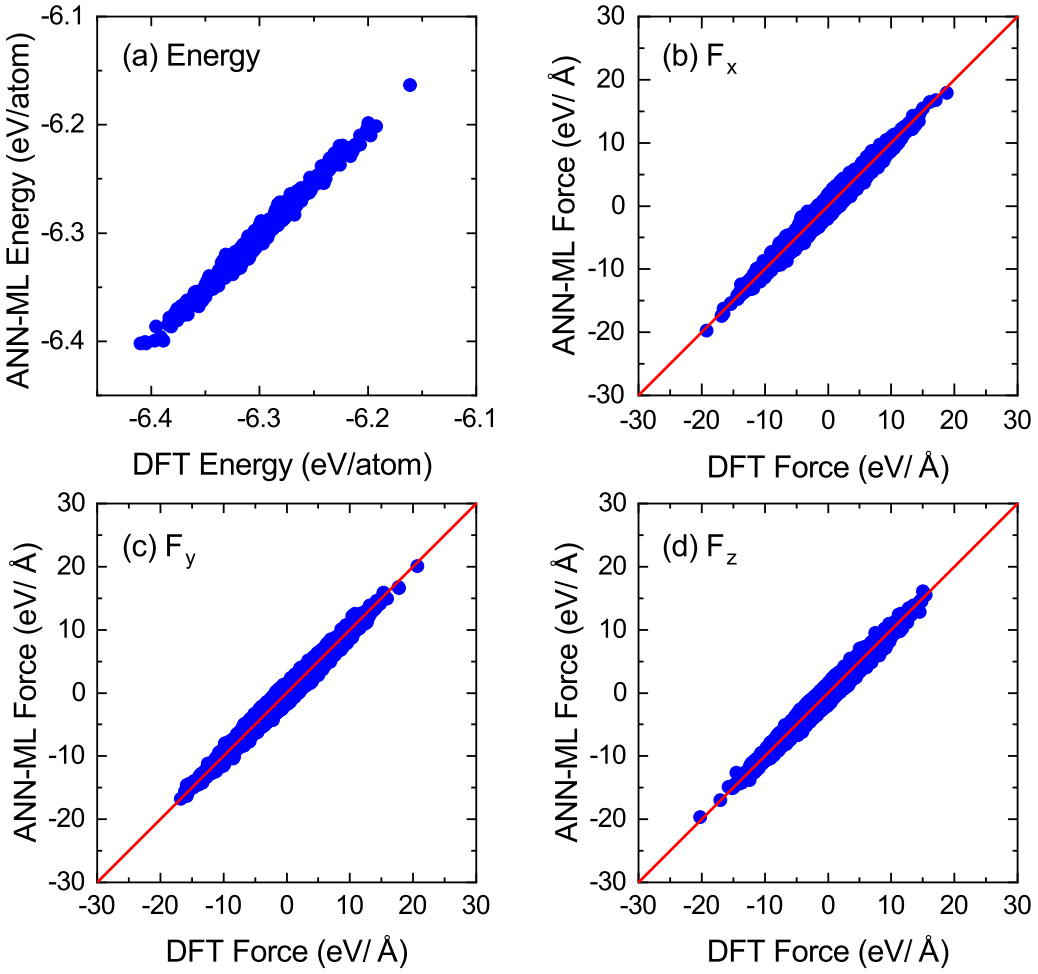

FIG. 2. Artificial neural-network machine learning (ANN-ML) vs density functional theory (DFT) energies and forces for the validation dataset of $Fe_{189}Si_{38}O_{23}$.

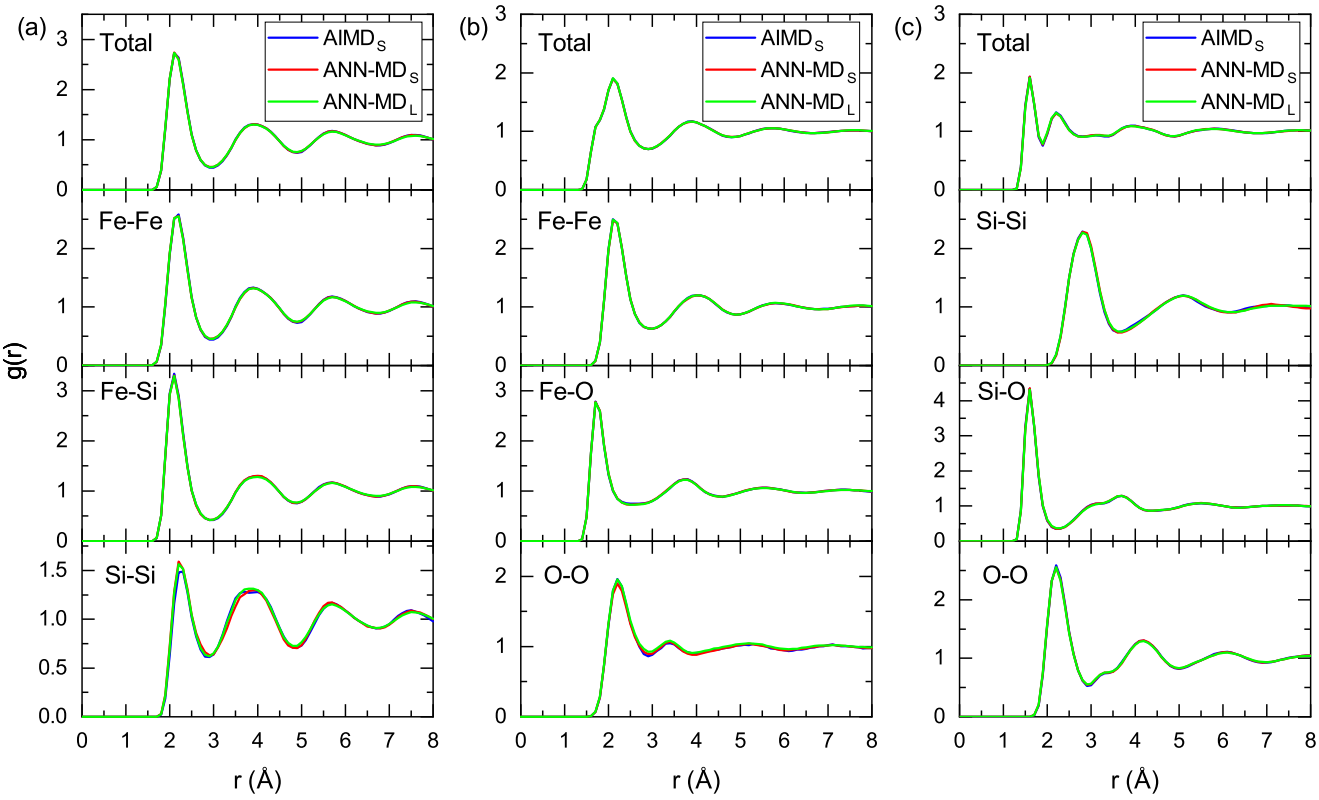

FIG. 3. Total and partial pair correlation functions of liquid (a) $Fe_{189}Si_{61}$, (b) $Fe_{189}O_{61}$, and (c) $Si_{80}O_{160}$ at 3800 K.

The AIMD simulations are performed using Vienna *Ab initio* Simulation Package (VASP) [4,43]. Projector augmented waves with the Perdew-Burke-Ernzerhof form of exchange-correlation potentials are adopted [44,45]. Only the Γ point is utilized to sample the Brillouin zone, and the default energy cutoffs of 400 eV are employed. The AIMD simulations are carried out using the NVT ensemble with a Nóse-Hoover thermostat under periodic boundary conditions. The time step of the AIMD simulations is 3 fs. A total of 124 455 snapshot structures with several different compositions from the AIMD have been collected for ML training, as can be seen from Table I. The AIMD simulations for each Fe-Si-O system to collect the snapshots for ML are performed at 3800, 4000, 4300, and 4800 K. At each temperature, the AIMD simulations for each system are performed at least with two different densities in the range specified in Table I. More details of training datasets are listed in Table S1 in the Supplemental Material [46].

Figure 2 shows the comparison of total potential energies and forces on each atom from the trained ANN-ML potential and *ab initio* calculated results for $Fe_{189}Si_{38}O_{23}$ liquid. The energies and forces predicted by the ANN-ML model and calculated by the *ab initio* method are plotted in the same figure as vertical and horizontal coordinates, respectively. The root mean square error (RMSE) of energy is ∼5.3 meV/atom, and the force RMSE is ∼0.43 eV/Å for the validation data. The training accuracy for other systems listed in Table I is like the one shown in Fig. 2. In comparison with the *ab initio* DFT calculation results, the relative error in energy and force from the ANN-ML potential prediction is ∼1 and 4%, respectively.

III. MD SIMULATION OF Fe-Si, Fe-O, AND Si-O BINARY LIQUIDS

With the interface of the DEEPMD-KIT to the LAMMPS code [47], MD simulations can be directly performed with the generated ANN-ML potential [29]. We first validate the reliability of the developed ANN-ML potential by comparing the structures and dynamics of $Fe_{189}Si_{61}$, $Fe_{189}O_{61}$, and $Si_{80}O_{160}$ liquids obtained from the MD simulations using the developed ANN-ML potential with those from AIMD simulations. The MD simulations by the ANN-ML potential are performed using a NVT ensemble and a Nóse-Hoover thermostat. Small and large simulation cells are used in the ANN-ML potential MD simulations. For the small simulation cell, the same box length as in the AIMD simulation is used. The large cell is a 2 × 2 × 2 supercell of the small one; thus, the densities of the small and large cells are the same. Periodic boundary conditions are applied in the three directions, and the time step of the simulations is 3 fs. According to the size of the simulation cell, we refer to a small simulation cell of 200–256 atoms as S and a large simulation cell of 2000–5000 atoms as L. For example, the AIMD$_S$ model of the $Fe_{189}Si_{38}O_{23}$ system contains 240 atoms, whereas the ANN-MD$_L$ model of the $Fe_{189}Si_{38}O_{23}$ system contains 2000 atoms. The same simulation conditions are applied, i.e., initial configurations, simulation steps, and NVT ensemble, on AIMD$_S$ and ANN-MD$_S$ models. The density of the studied $Fe_{189}Si_{61}$, $Fe_{189}O_{61}$, and $Si_{80}O_{160}$ liquids in this section are 9.78, 9.57, and 5.31 g/cm^3 at 3800 K, respectively. The pressures obtained from the ANN-MD$_S$ and ANN-MD$_L$ models are almost the same but are ∼ 6.8–10.1% larger than that from the AIMD$_S$ model. The pressures of

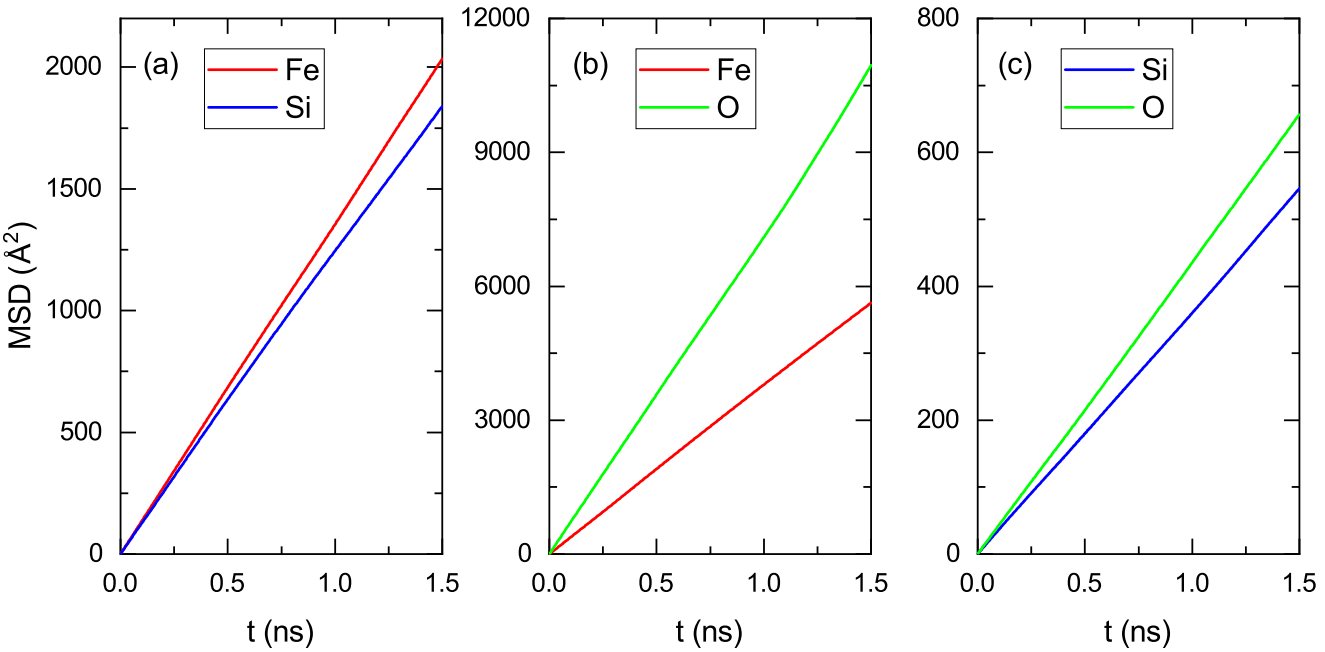

FIG. 4. Mean square displacement of (a) $Fe_{189}Si_{61}$, (b) $Fe_{189}O_{61}$, and (c) $Si_{80}O_{160}$ liquid from the ANN-MD_L model at 3800 K.

the $Fe_{189}Si_{61}$, $Fe_{189}O_{61}$, and $Si_{80}O_{160}$ liquids are 135 (144), 134 (147), and 133 (143) GPa from the $AIMD_S$ (ANN-MD_S) model at 3800 K, respectively.

The structures of the $Fe_{189}Si_{61}$, $Fe_{189}O_{61}$, and $Si_{80}O_{160}$ liquids at 3800 K are analyzed from the $AIMD_S$, ANN-MD_S, and ANN-MD_L models. Pair correlation functions (PCFs) are calculated to quantitatively describe the structure of liquids. The PCF $g(r)$ is a conditional probability density of finding a particle at distance r, given that there is a particle at the coordinate origin. Thus, $g(r)$ provides a measure of local spatial ordering in a liquid. Mathematically, the partial PCF between the atom types α and β is given by $g_{\alpha\beta}(r) = \rho_{\alpha\beta}^{-2}\langle\sum_i\sum_{j\neq i}\delta(\vec{r}_{i\alpha})\delta(\vec{r}_{j\beta}-r)\rangle$, where $\rho_{\alpha\beta} = \rho_0\sqrt{a_\alpha a_\beta}$ corresponds to a partial density with ρ_0 being the atomic density

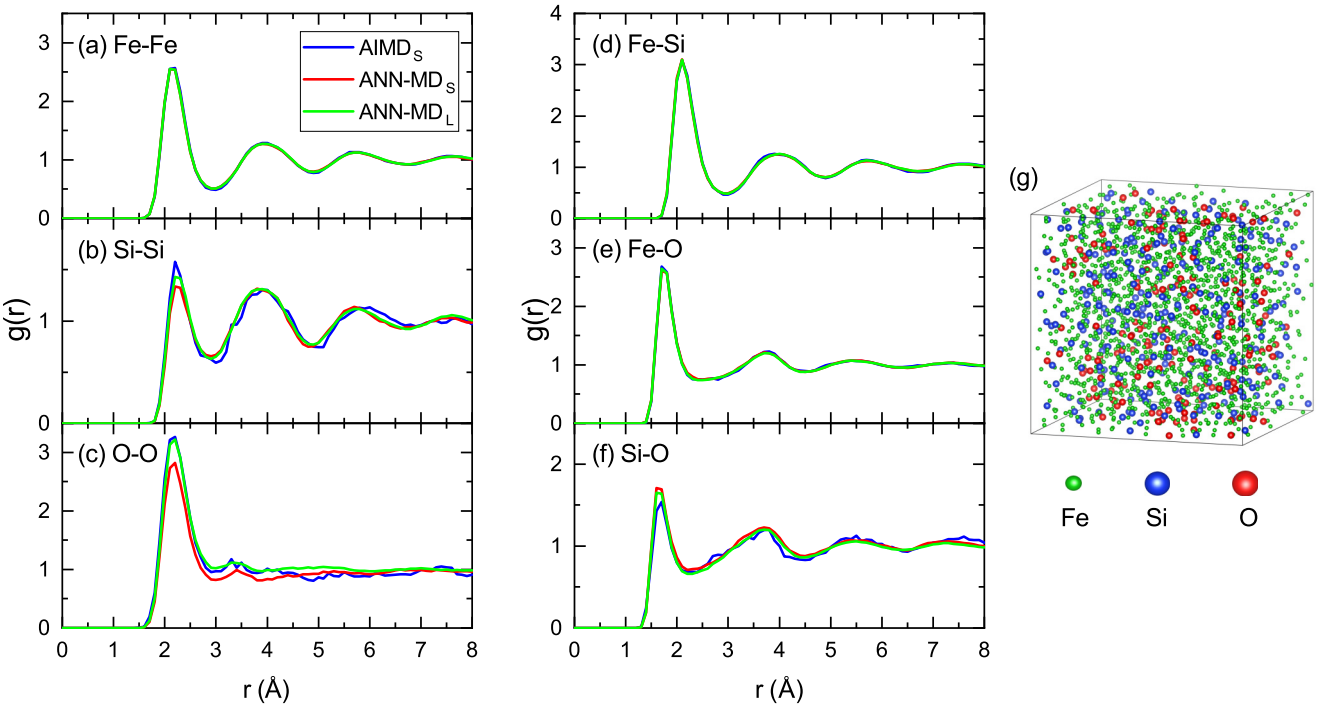

FIG. 5. (a)–(f) Partial pair correlation functions of liquid $Fe_{189}Si_{38}O_{23}$ at 3800 K. (g) Snapshot of $Fe_{189}Si_{38}O_{23}$ liquid from the ANN-MD_L model at 3800 K and 145 GPa at 3.0 ns.

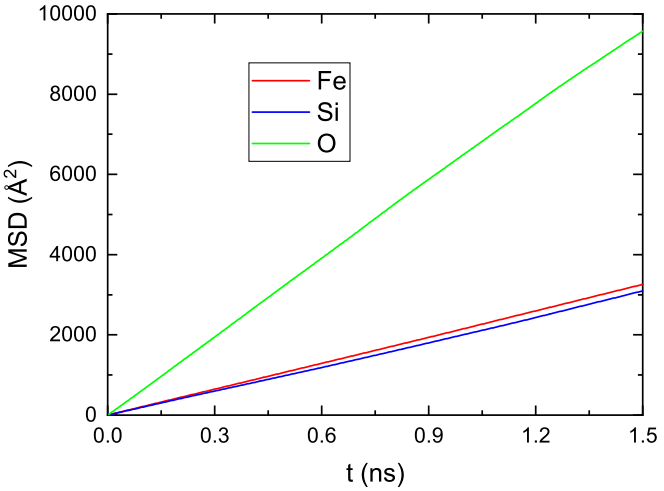

FIG. 6. Mean square displacement of liquid $Fe_{189}Si_{38}O_{23}$ at 3800 K from the ANN-MD_L model.

of the liquid and a_α and a_β being the atomic concentrations of the corresponding elements in the liquid [48]. The total and partial PCFs of the liquid from our simulations are shown in Fig. 3. The PCFs of binary $Fe_{189}Si_{61}$, $Fe_{189}O_{61}$, and $Si_{80}O_{160}$ liquids at 3800 K obtained by AIMD and ANN-MD agree well with each other. For the $Fe_{189}Si_{61}$ binary system, the positions of the first peak of partial PCFs of Fe-Fe, Fe-Si, and Si-Si are ∼2.2, 2.1, and 2.2 Å, respectively. These results indicate that the nearest-neighbor distances between Fe and Si atoms and among the Fe or Si atoms themselves in $Fe_{189}Si_{61}$ binary liquid are very similar, which is in good agreement with previous works [49,50]. For the $Fe_{189}O_{61}$ binary system, the first PCF peak of O-O is 2.2 Å, which is significantly larger than Fe-O (1.7 Å) and Fe-Fe (2.1 Å). This indicates that O atoms do not form the nearest-neighbor bonds among themselves in the liquid Fe-O system. The first PCF peak of O-O in the $Si_{80}O_{160}$ binary system is also 2.2 Å, which stands as the median of Si-Si (2.8 Å) and Si-O (1.6 Å). It is noteworthy that the bond length of O-O in the $Si_{80}O_{160}$ system is the same to that in the $Fe_{189}O_{61}$ system, indicating that O atoms also do not form the nearest-neighbor bonds among themselves in the liquid Si-O system. In addition to the PCF, the partial angular distribution functions (ADFs) can provide more local structural information about the liquid samples. The ADFs obtained from AIMD and ANN-MD coincide with each other, as shown in the Supplemental Material [46], which further indicates the reliability of the ANN-ML potential. Excellent agreement of PCFs and ADFs is also observed for AIMD with small (ANN-MD_S) and large (ANN-MD_L) simulation cells, therefore confirming the validation of the ANN-ML potential for large systems. Thanks to the local decomposition and the near-neighbor dependence of the atomic energies, the ANN-ML potential trained on a relatively small system can be used to investigate a bigger system, as discussed above. We compared the computational time per MD step in AIMD and the inference time per MD step in ANN-MD for the SiO_2 liquid with different system sizes, as shown in Fig. S1 in the Supplemental Material [46]. The results show that the inference time of the ANN-MD scales linearly with the number of atoms and would be $\sim 10^5$ times faster than AIMD for a system with 5000 atoms, which is consistent with previous studies [30,35].

To quantitatively study the dynamic properties, we calculated the self-diffusion constants D of every element in the

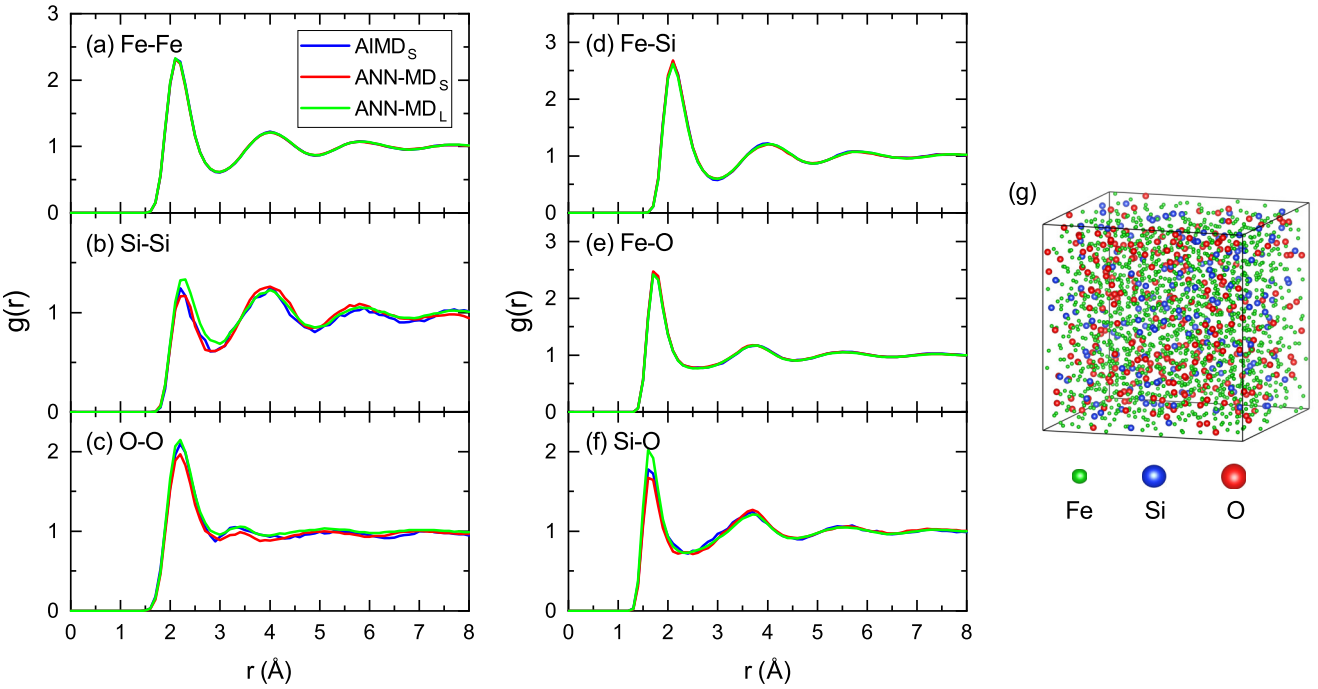

FIG. 7. (a)–(f) Partial pair correlation functions of $Fe_{189}Si_{23}O_{38}$ liquid at 4800 K. (g) Snapshot of $Fe_{189}Si_{38}O_{23}$ liquid from ANN-MD_L at 4800 K and 145 GPa at 3.0 ns. The *ab initio* molecular dynamics (AIMD) snapshots of $Fe_{189}Si_{38}O_{23}$ liquid are not used in the artificial neural-network machine learning (ANN-ML) training.

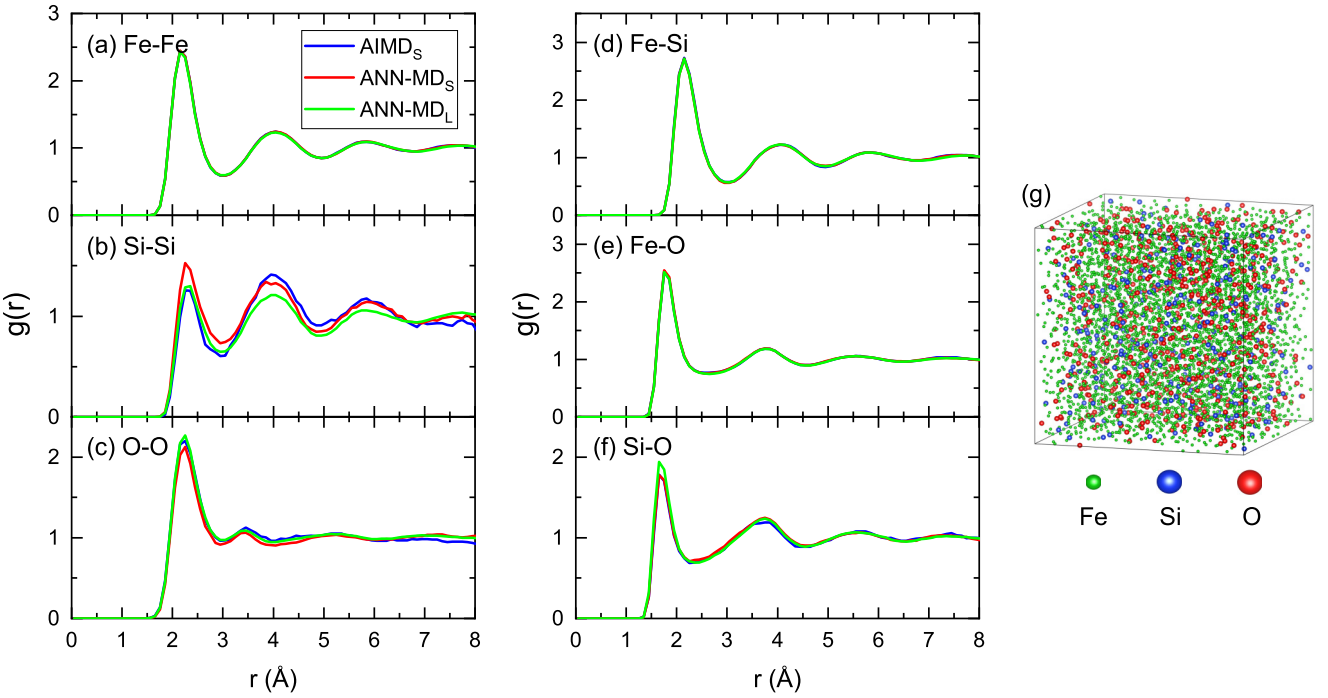

FIG. 8. (a)–(f) Partial pair correlation functions of $Fe_{158}Si_{14}O_{28}$ liquid at 4500 K. (g) Snapshot of $Fe_{158}Si_{14}O_{28}$ liquid from ANN-MD$_L$ at 4500 K and 148 GPa at 20 ps. The *ab initio* molecular dynamics (AIMD) snapshots of $Fe_{158}Si_{14}O_{28}$ liquid are not used in the artificial neural-network machine learning (ANN-ML) training.

binary liquids. The mean squared displacement (MSD) as a function of time is given by [48,51]

$$\left\langle R_\alpha^2(t)\right\rangle = \frac{1}{N_\alpha}\left\langle \sum_{i=1}^{N_\alpha} |R_{i\alpha}(t+\tau) - R_{i\alpha}(\tau)|^2 \right\rangle,$$

where N_α is the total atomic number of α species, $R_{i\alpha}$ is the coordinates of the atom i, and τ is the arbitrary origin of time. The MSD of the liquids in the limit of long time should behave linearly with the time, and the slope of the line gives the self-diffusion constant D by the Einstein relationship:

$$D = \lim_{t\to\infty} \left\langle R_{i\alpha}^2(t)\right\rangle / 6t.$$

The self-diffusion constants D of $Fe_{189}Si_{61}$, $Fe_{189}O_{61}$, and $Si_{80}O_{160}$ binary systems are calculated within 1.5 ns from the ANN-MD$_L$ models, as shown in Fig. 4. For the $Fe_{189}Si_{61}$ binary system, Fe and Si have similar diffusing constant, i.e., $D_{Fe} = 0.26 \times 10^{-8} m^2/s$ and $D_{Si} = 0.20 \times 10^{-8} m^2/s$. The diffusion constants of Fe and O in the $Fe_{189}O_{61}$ binary system are $D_{Fe} = 0.63 \times 10^{-8} m^2/s$ and $D_O = 1.20 \times 10^{-8} m^2/s$, respectively, which means O atoms move faster than Fe atoms in the $Fe_{189}O_{61}$ system. The diffusion constants of Si and O in the $Si_{80}O_{160}$ binary system are $D_{Si} = 0.60 \times 10^{-8} m^2/s$ and $D_O = 0.73 \times 10^{-8} m^2/s$, respectively. These data agree with those obtained from liquid Fe and Fe-O under Earth's outer core conditions [50,52–56].

IV. MD SIMULATION OF Fe-Si-O TERNARY LIQUIDS

A. Validation of ANN-ML potential for $Fe_{189}Si_{38}O_{23}$ ternary liquid

We performed MD simulation of the $Fe_{189}Si_{38}O_{23}$ ternary system with density of 9.91 g/cm^3 at 3800 K. The pressures of the $Fe_{189}Si_{38}O_{23}$ liquid at 3800 K are 132, 145, and 145 GPa from AIMD$_S$, ANN-MD$_S$, and ANN-MD$_L$ models, respectively. The partial PCFs of the $Fe_{189}Si_{38}O_{23}$ ternary system at 3800 K from AIMD$_S$, ANN-MD$_S$, and ANN-MD$_L$ models are shown in Fig. 5. The partial PCF distributions from AIMD$_S$, ANN-MD$_S$, and ANN-MD$_L$ models are similar, especially the peak positions. This further indicates the validation of the ANN-ML potential for ternary systems. The first peak of the O-O partial PCF is located at 2.2 Å, whereas the positions of the first peak of Fe-O and Si-O are both 1.7 Å. This indicates O atoms do not form nearest-neighbor bonds among themselves in the Fe-Si-O ternary system. The bond lengths of O-O, Fe-O, and Si-O in the $Fe_{189}Si_{38}O_{23}$ ternary system are like those in $Fe_{189}O_{61}$ and $Si_{80}O_{160}$ binary systems. The bond lengths of Fe-Fe, Si-Si, and Fe-Si in the $Fe_{189}Si_{38}O_{23}$ ternary system are 2.2, 2.2, and 2.1 Å, respectively, which are like that in the $Fe_{189}Si_{61}$ binary system. In addition, the potential energy fluctuates around a constant value with MD simulation time, indicating no phase transition or separation takes place at 3800 K, as shown in the Supplemental Material [46]. Figure 5(g) shows that Fe, Si, and O atoms are mixed well with each other. This indicates there is no phase separation in the Fe-Si-O system and no immiscibility between Fe-Si and Fe-Si-O liquids at 3800 K, which is consistent with previous work [50].

The self-diffusion constant D of the $Fe_{189}Si_{38}O_{23}$ ternary system at 3800 K is calculated within 1.5 ns from the ANN-MD_L model, as shown in Fig. 6. We find $D_{Fe} = 0.36 \times 10^{-8} m^2/s$, $D_{Si} = 0.34 \times 10^{-8} m^2/s$, and $D_O = 1.07 \times 10^{-8} m^2/s$. The self-diffusion constants of Fe and Si in the $Fe_{189}Si_{38}O_{23}$ ternary system are similar, which is also found in the $Fe_{189}O_{61}$ binary system. D_O is ~3 times D_{Fe} or D_{Si}, which is consistent with previous work [50].

B. Further test of ANN-ML potential for $Fe_{189}Si_{23}O_{38}$ and $Fe_{158}Si_{14}O_{28}$ ternary liquids

In addition to the $Fe_{189}Si_{38}O_{23}$ ternary system at 3800 K whose AIMD snapshots have been used in the training data for the ANN-ML potential, we also performed MD simulations for liquid $Fe_{189}Si_{23}O_{38}$ and $Fe_{158}Si_{14}O_{28}$ ternary systems (whose AIMD snapshots are not used in the ANN-ML training) to further test the accuracy and transferability of the obtained ANN-ML potential for Fe-Si-O systems with O richer than Si.

The density of $Fe_{189}Si_{23}O_{38}$ liquid at 4800 K is 9.85 g/cm^3 for the $AIMD_S$, ANN-MD_S, and ANN-MD_L models, whereas the pressures are 132, 143, and 143 GPa from the three models, respectively. The partial PCF of the $Fe_{189}Si_{23}O_{38}$ from the ANN-MD_S model (250 atoms) agrees well with that from the $AIMD_S$ model (250 atoms), as shown in Fig. 7. From Fig. 7(g), we can see that Fe, Si, and O atoms mix well with each other, which means no phase separation in the $Fe_{189}Si_{23}O_{38}$ ternary system.

The density of $Fe_{158}Si_{14}O_{28}$ liquid at 4500 K is 10.16 g/cm^3 for the $AIMD_S$, ANN-MD_S, and ANN-MD_L models, whereas the pressures are 136, 148, and 148 GPa from the three models, respectively. The partial PCF of $Fe_{158}Si_{14}O_{28}$ from the $AIMD_S$ model (200 atoms) agrees well with that from the ANN-MD_S and ANN-MD_L models (5000 atoms), as shown in Fig. 8. The efficiency of the ANN-ML potential enables MD simulations with a larger unit cell to be compared with the results from the small (200 atoms) unit cell. From Fig. 8(g), we can see that Fe, Si, and O atoms mix well with each other, which means no phase separation in the $Fe_{158}Si_{14}O_{28}$ ternary system. The reliability of the ANN-ML potential is further tested on $Fe_{158}Si_{42}$ at 4500 K and pure Fe at 3500 K. We note that the structures of $Fe_{158}Si_{42}$ liquid are not included in the training dataset, while the AIMD snapshots of Fe are included in the training dataset. The PCFs of the two systems are shown in the Supplemental Material [46]. The PCFs of $Fe_{158}Si_{42}$ and Fe from AIMD and ANN-MD agree with each other.

V. SUMMARY

In this paper, we have developed an ANN-ML potential for the Fe-Si-O system at the high-pressure and high-temperature conditions of the Earth's outer core using the DEEPMD-KIT and VASP software packages. The developed ANN-ML potential can be used in the LAMMPS package to perform MD simulations. The ANN-ML potential not only can reproduce well the AIMD results on structures of the binary and ternary liquids whose snapshot structures were included in the ANN-ML training dataset but also provide consistent MD simulation results of ternary liquids ($Fe_{189}Si_{23}O_{38}$ and $Fe_{158}Si_{14}O_{28}$) whose snapshot structures were not included in the training dataset. The results show there is no phase separation and exsolution in our studied three ternary systems ($Fe_{189}Si_{38}O_{23}$, $Fe_{189}Si_{23}O_{38}$, and $Fe_{158}Si_{14}O_{28}$) ~ 136 GPa. More training data and larger neural network size would help to further improve the accuracy and transferability of the ANN-ML interatomic potential of the Fe-Si-O system. Our results suggest the ANN-ML potential would be a promising avenue for MD simulation of complex Fe-Si-O systems under the Earth's outer core conditions.

ACKNOWLEDGMENTS

C.Z. was supported by the National Natural Science Foundation of China (Grants No. 11874318 and No. 11774299) and the Natural Science Foundation of Shandong Province (Grants No. ZR2018MA043 and No. ZR2017MA033). L.T. acknowledges the support by the National Natural Science Foundation of China (Grant No. 11304279). Y.S. was supported by U.S. National Science Foundation (NSF) Awards No. EAR-1918134 and No. EAR-1918126. K.M.H. and C. Z. Wang were supported by US NSF Award No. EAR-1918134. R.M.W. was supported by US NSF Award No. EAR-1918126.

[1] D. Frenkel and B. Smit, *Understanding Molecular Simulation: From Algorithms to Applications* (Academic Press, Orlando, 2002).
[2] D. C. Rapaport, *The Art of Molecular Dynamics Simulation* (Cambridge University Press, Cambridge, 2004).
[3] R. Car and M. Parrinello, Phys. Rev. Lett. **55**, 2471 (1985).
[4] G. Kresse and J. Hafner, Phys. Rev. B **47**, 558 (1993).
[5] R. Zwanzig, J. Chem. Phys. **22**, 1420 (1954).
[6] L. Verlet, Phys. Rev. **159**, 98 (1967).
[7] J. Tersoff, Phys. Rev. B **39**, 5566 (1989).
[8] R. L. C. Vink, G. T. Barkema, W. F. van der Weg, and N. Mousseau, J. Non-Cryst. Solids **282**, 248 (2001).
[9] M. S. Daw and M. I. Baskes, Phys. Rev. B **29**, 6443 (1984).
[10] Y. Q. Cheng and E. Ma, Prog. Mater. Sci. **56**, 379 (2011).
[11] H. W. Sheng, E. Ma, and M. J. Kramer, JOM **64**, 856 (2012).
[12] D. J. Hepburn and G. J. Ackland, Phys. Rev. B **78**, 165115 (2008).
[13] J. Behler and M. Parrinello, Phys. Rev. Lett. **98**, 146401 (2007).
[14] N. Artrith and A. Urban, Compt. Mater. Sci. **114**, 135 (2016).
[15] A. P. Bartók and G. Csányi, Int. J. Quantum. Chem. **115**, 1051 (2015).
[16] A. P. Bartók, J. R. Kermode, N. Bernstein, and G. Csányi, Phys. Rev. X **8**, 041048 (2018).
[17] C. Chen, Z. Deng, R. Tran, H. Tang, I.-H. Chu, and S. P. Ong, Phys. Rev. Materials **1**, 043603 (2017).

[18] Z. Deng, C. Chen, X.-G. Li, and S. P. Ong, npj Comput. Mater. **5**, 75 (2019).

[19] D. Dragoni, T. D. Daff, G. Csányi, and N. Marzari, Phys. Rev. Materials **2**, 013808 (2018).

[20] S. Faraji, S. A. Ghasemi, S. Rostami, R. Rasoulkhani, B. Schaefer, S. Goedecker, and M. Amsler, Phys. Rev. B **95**, 104105 (2017).

[21] K. Gubaev, E. V. Podryabinkin, G. L. W. Hart, and A. V. Shapeev, Compt. Mater. Sci. **156**, 148 (2019).

[22] T. S. Hy, S. Trivedi, H. Pan, B. M. Anderson, and R. Kondor, J. Chem. Phys. **148**, 241745 (2018).

[23] R. Z. Khaliullin, H. Eshet, T. D. Kühne, J. Behler, and M. Parrinello, Nat. Mater. **10**, 693 (2011).

[24] X.-G. Li, C. Hu, C. Chen, Z. Deng, J. Luo, and S. P. Ong, Phys. Rev. B **98**, 094104 (2018).

[25] E. V. Podryabinkin and A. V. Shapeev, Compt. Mater. Sci. **140**, 171 (2017).

[26] K. T. Schütt, P. Kessel, M. Gastegger, K. A. Nicoli, A. Tkatchenko, and K. R. Müller, J. Chem. Theory Comput. **15**, 448 (2019).

[27] K. T. Schütt, H. E. Sauceda, P. J. Kindermans, A. Tkatchenko, and K. R. Müller, J. Chem. Phys. **148**, 241722 (2018).

[28] A. V. Shapeev, Multiscale Model. Simul. **14**, 1153 (2016).

[29] H. Wang, L. Zhang, J. Han, and W. E., Comput. Phys. Commun. **228**, 178 (2018).

[30] L. Zhang, J. Han, H. Wang, R. Car, and W. E., Phys. Rev. Lett. **120**, 143001 (2018).

[31] L. Zhang, J. Han, H. Wang, W. Saidi, R. Car, and W. E., in *Advances in Neural Information Processing Systems 31* (NeurIPS, 2018).

[32] L. Zhang, D.-Y. Lin, H. Wang, R. Car, and W. E., Phys. Rev. Materials **3**, 023804 (2019).

[33] Y. Zuo, C. Chen, X. Li, Z. Deng, Y. Chen, J. Behler, G. Csányi, A. V. Shapeev, A. P. Thompson, M. A. Wood, and S. P. Ong, J. Phys. Chem. A **124**, 731 (2020).

[34] L. Tang, K. M. Ho, and C. Z. Wang, J. Chem. Phys. **155**, 194503 (2021).

[35] L. Tang, Z. J. Yang, T. Q. Wen, K. M. Ho, M. J. Kramer, and C. Z. Wang, Phys. Chem. Chem. Phys **22**, 18467 (2020).

[36] L. Tang, Z. J. Yang, T. Q. Wen, K. M. Ho, M. J. Kramer, and C. Z. Wang, Acta Mater. **204**, 116513 (2021).

[37] T. Wen, C.-Z. Wang, M. J. Kramer, Y. Sun, B. Ye, H. Wang, X. Liu, C. Zhang, F. Zhang, K.-M. Ho, and N. Wang, Phys. Rev. B **100**, 174101 (2019).

[38] C. Zhang, Y. Sun, H.-D. Wang, F. Zhang, T.-Q. Wen, K.-M. Ho, and C.-Z. Wang, J. Phys. Chem. C **125**, 3127 (2021).

[39] J. Wang, H. Shen, R. Yang, K. Xie, C. Zhang, L. Chen, K.-M. Ho, C.-Z. Wang, and S. Wang, Carbon **186**, 1 (2022).

[40] K. Xie, C. Qiao, H. Shen, R. Yang, M. Xu, C. Zhang, Y. Zheng, R. Zhang, L. Chen, K.-M. Ho, C.-Z. Wang, and S. Wang, J. Phys.:Condens. Matter **34**, 075402 (2022).

[41] D. P. Kingma and J. Ba, in *International Conference on Learning Representations* (ICLR, San Diego, 2015).

[42] K. He, X. Zhang, S. Ren, and J. Sun, in *IEEE Conference on Computer Vision and Pattern Recognition* (IEEE, Las Vegas, 2016), p. 770.

[43] G. Kresse and J. Furthmüller, Phys. Rev. B **54**, 11169 (1996).

[44] P. E. Blöchl, Phys. Rev. B **50**, 17953 (1994).

[45] J. P. Perdew, K. Burke, and M. Ernzerhof, Phys. Rev. Lett. **77**, 3865 (1996).

[46] See Supplemental Material at http://link.aps.org/supplemental/10.1103/PhysRevMaterials.6.063802 for data format of DEEPMD-KIT, computational time comparison, training and validation datasets, bond angle distributions of binary systems, potential energy vs MD times of tenary system, PCFs of liquid Fe, and PCFs of liquid $Fe_{158}Si_{42}$.

[47] S. Plimpton, J. Comput. Phys. **117**, 1 (1995).

[48] S. Y. Wang, M. J. Kramer, M. Xu, S. Wu, S. G. Hao, D. J. Sordelet, K. M. Ho, and C. Z. Wang, Phys. Rev. B **79**, 144205 (2009).

[49] J. Brodholt and J. Badro, Geophys. Res. Lett. **44**, 8303 (2017).

[50] D. Huang, J. Badro, J. Brodholt, and Y. Li, Geophys. Res. Lett. **46**, 6397 (2019).

[51] X. W. Fang, C. Z. Wang, Y. X. Yao, Z. J. Ding, and K. M. Ho, J. Phys.:Condens. Matter **23**, 235104 (2011).

[52] L. Vočadlo, G. A. de Wijs, G. Kresse, M. Gillan, and G. D. Price, Farad. Discuss. **106**, 205 (1997).

[53] D. Alfè, G. D. Price, and M. J. Gillan, Phys. Earth Planet. Inter. **110**, 191 (1999).

[54] M. Pozzo, C. Davies, D. Gubbins, and D. Alfè, Phys. Rev. B **87**, 014110 (2013).

[55] E. S. Posner, D. C. Rubie, D. J. Frost, V. Vlček, and G. Steinle-Neumann, Geochim. Cosmochim. Acta **203**, 323 (2017).

[56] E. S. Posner, G. Steinle-Neumann, V. Vlček, and D. C. Rubie, Geophys. Res. Lett. **44**, 3526 (2017).